Identification of the Flow Structures and Regime Transition in Gas–Solid Fluidized Beds Through Moment Analysis

Jesse Zhu, Maozhan Qi, and Shahzad Barghi
Dept. of Chemical and Biochemical Engineering, University of Western Ontario, London, Ontario, Canada N6A 5B9

DOI 10.1002/aic.13948
Published online November 13, 2012 in Wiley Online Library (wileyonlinelibrary.com).

Using statistic parameters of solids holdup signals, a moment consistency data processing method (MCDPM) was proposed. Experiments were carried out using FCC particles of 76 μm under different operating conditions, and MCDPM was used to successfully obtain solids holdups of the dense and dilute phases and the phase fractions over five fluidization regimes, bubbling (BFB), turbulent (TFB), circulating turbulent (CTFB), high-density circulating (HDCFB), and circulating (CFB) fluidized bed systems. In BFB, TFB, and CTFB regimes, only dense phase fraction decreased with increasing air velocity, while the transition from HDCFB to CFB experienced appreciable change in the solids holdup of the dense phase. From the low-velocity to the high-velocity regimes, both the solids holdup and the fraction of the dense phase experienced a drastic decrease, suggesting that this transition corresponded to a profound change in flow structure and further suggesting that CTFB is in reality still a TFB. © 2012 American Institute of Chemical Engineers *AIChE J,* 59: 1479–1490, 2013
Keywords: moment analysis, phase division, flow structure, gas–solid fluidization, modeling, data processing

Introduction

Many industrial processes have been utilizing gas–solid fluidized bed reactors that may operate in the following flow regimes: particulate fluidization, bubbling fluidization, turbulent fluidization, fast fluidization, and pneumatic transport.[1,2] (It should be noted that the term turbulent as used here refers to a fluidization regime as originally proposed by Kehoe and Davidson[3] and widely accepted by the fluidization community, not to the multiphase flow behavior in terms of fluid mechanics. As a matter of fact, the flow in all fluidized beds is turbulent in term of fluid mechanics.) Among the industrial applications of these fluidized beds, most key commercial gas–solid fluidized bed reactors operate in the flow regimes of turbulent fluidization (turbulent fluidized bed, TFB) and fast fluidization (circulating fluidized bed, CFB) due to their favorable gas–solid contacting, mixing, and transfer characteristics. They include not only catalytic cracking, partial oxidation reactions, chlorination, and so forth but also some important noncatalytic processes, such as roasting of various ores and drying.[1,4] Among these fluidized bed reactors, typical fluid catalytic cracking (FCC) units are operated under high-density circulating fluidization (high-density circulating fluidized bed, HDCFB) conditions, at high gas velocities from 6 to 28 m/s and high solids circulation rates from 400 to 1200 kg/(m^2s) with high solids holdups of typically 10–20%.[5] Fischer–Tropsch synthesis and acrylonitrile production routinely operate in the turbulent regime of fluidization, for which heat and mass transfer tend to reach a maximum.[6] For these operations, fluidized beds are able to operate with small catalyst particles and hence high effectiveness factors, favorable bed-to-immersed-surface heat transfer coefficients in CFB and TFB reactors. They are also capable of withdrawing and adding particulate solids continuously and operating on a very large scale.[7]

Gas–solid fluidized beds are commonly classified as low-velocity and high-velocity fluidized beds.[5,6] Furthermore, low-velocity beds are further classified into fluidization regimes of bubbling fluidized bed (BFB), TFB, and circulating turbulent fluidized bed (CTFB),[1,8] whereas the high-velocity beds are studied in HDCFB and CFB regimes.[5] Due to different air velocities and different levels of interaction between gas and solid phases,[9,10] fluidized beds have been characterized by their heterogeneous two-phase flow structures. Typically, BFB has dense phase flow structure with dispersed bubbles, whereas HDCFB and CFB have dilute flow structure with dispersed clusters. TFB and CTFB, which may be regarded as transition fluidization regimes between BFB and CFB,[10,11] have competing flow structures between dilute and dense phases. On the other hand, the heterogeneous flow structures are investigated macroscopically and microscopically to understand gas–solid fluidized bed reactors. The macroscopic flow structure usually refers to radial and axial distribution of solids holdup and particle velocity throughout the beds,[7,12] whereas the microscopic flow structure refers to the localized behavior of the dense and dilute phases.[9,13]

The heterogeneous flow structures in fluidized beds are attributed to many physical factors of the flow systems, such as gas flow behavior, particle property, density difference between gas and solids, various interactive forces between gas and solids, bed geometry and gas distribution, and so forth. Theoretically, these effects on the flow structure should be identified individually and/or modeled by CFD

Correspondence concerning this article should be addressed to J. Zhu at jzhu@uwo.ca.

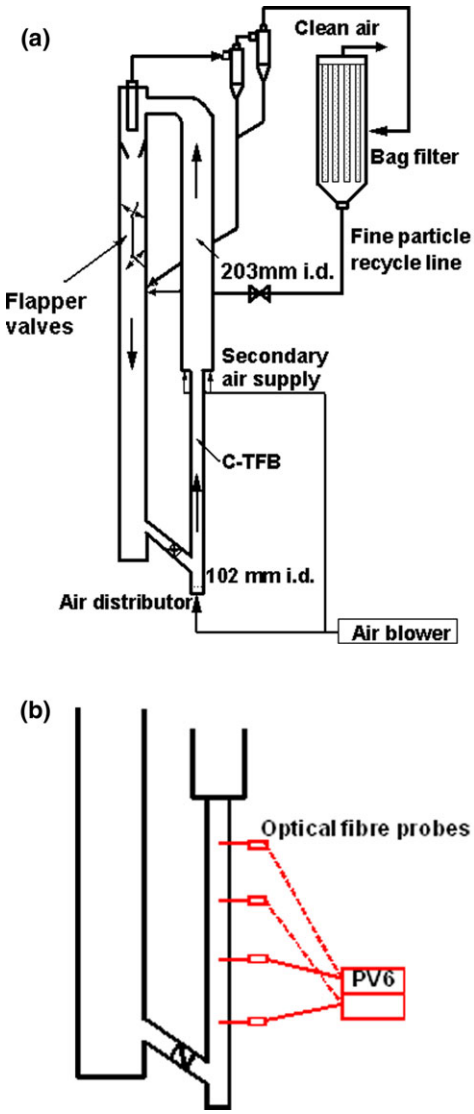

Figure 1. (a) Experimental apparatus setup. (b) Optical fiber probe setup.

[Color figure can be viewed in the online issue, which is available at wileyonlinelibrary.com.]

and other methods, but such efforts have led to very limited success due to the complicated relationships to be understood.[14] Therefore, other methods have been proposed to mathematically characterize the flow structures inside the various fluidized beds, such as the time series analysis through chaos method[15,16] and moment method.[17] The moment analysis method uses some or all of the four moments of the local solids holdup signals. The first moment (mean value) corresponds to the local time average solids holdup, and the second moment (standard deviation) relates to the fluctuations of the solids holdup around the mean value,[12,13,18] reflecting the heterogeneity of a gas–solid flow. The third moment (skewness) is a measure of the lack of symmetry in the probability density function (PDF) of the solids holdup around the mean. The fourth moment (kurtosis) is a measure of the peakedness or flatness of PDF of the solids holdup compared to a normal distribution.[13,17,19,20] Despite their importance, skewness and kurtosis have not been very often used in analyzing the hydrodynamics of fluidization systems. Using the skewness of local solids signals, Manyele et al.[21] analyzed the hydrodynamics of a downer reactor and concluded that skewness provides more information that could not be identified directly from the PDFs. Using all four moments, Bi and Su[11] proposed a two-phase structural model to predict the average solids holdups and phase volume fractions of dense and dilute phases in some gas–solids fluidization and transport systems. Breault et al.[22] and Taylor et al.[17] investigated the hydrodynamics of upflow in a riser using direct wavelet transformation, skewness, and kurtosis.

The objective of this study is to apply a new moment analysis method, the moment consistency data processing method (MCDPM), to study the detailed flow structure on various flow regimes, and to identify distinct changes along with change of operating conditions and regime transition in gas–solid fluidization systems. Additionally, this method is used to further confirm the existence of a circulating turbulent fluidization regime with regard to its microscopic flow structure. Such a CTFB reactor was proposed by Zhu and Zhu,[7] integrating conventional CFB and TFB into a distinguished dense fluidization system with external solids circulation, to simultaneously achieve efficient gas–solid contact similar to TFB and low solids back-mixing similar to HDCFB. Their results demonstrated that the CTFB operation is achievable, and its flow structure can be attributed to a new flow regime, the circulating turbulent fluidization regime, independent of turbulent fluidization, fast fluidization, and dense suspension upflow.[2,9] Although our earlier studies[7,9] have utilized the first and second moments to distinguish and characterize the various fluidization regimes, more details of the dynamic flow structure, such as the division of the dense and dilute phases, may be further revealed through the additional application of the third and fourth moments.

Experimental Setup

Experiments were carried out in a CTFB and a twin riser fluidized bed, covering bubbling fluidization (BFB), turbulent fluidization (TFB), circulating turbulent fluidization (CTFB), fast fluidization (CFB), and high-density circulating fluidization regimes (HDCFB). The schematic diagram of the first experimental unit is shown in Figure 1, whose detail description can be found in Zhu and Zhu.[7] Steady flow of different fluidization regimes at low air velocities, namely, BFB, TFB, CTFB regimes, and bottom zone of CFB, were obtained through controlling the solids circulation rate and adjusting the air flow. Air velocities and solids circulation rates are listed in Table 1, corresponding to bubbling, circulating turbulent, and fast fluidization regimes at low air velocities.

Experimental data on solids concentration inside the various fluidized beds were acquired using fiber optical reflective probes of model PV-6, developed and manufactured by the Institute of Process Engineering, Chinese Academy of Sciences, Beijing, China.[23] The probe was set up at four axial

Table 1. Operating Conditions of Experiments

Regime	BFB*	TFB*	CTFB	HDCFB**	CFB**
D (mm)	102	102	102	76	203
Height (m)	3.6	3.6	3.6	10	10
d_p (μm)	76	76	76	67	67
ρ_p (kg/m^3)	1780	1780	1780	1500	1500
u_g (m/s)	0.53–0.74	1.6	0.74–3.0	5.5–10	5.5–8.0
G_s [kg/(m^{2}s)]	0	0	150–420	300–550	50–100

*Dynamic bed height of 3.6 m.
**Data from Yan and Zhu.[12]

elevations and traversed horizontally to measure local solids holdups at 11 radial positions (Figure 1b). The four axial locations were chosen in an effort to characterize the acceleration zone (0.8 m) and the fully developed zone (1.5, 2.2, and 3.0 m). Radial positions were chosen as the midpoints of 11 equal area circles (r/R = 0.0, 0.16, 0.38, 0.5, 0.59, 0.67, 0.74, 0.81, 0.87, 0.92, and 0.98) at each axial level within the risers. To ensure the consistency of the data at one specific operating condition, the data at all locations were collected within one run by the probe. The sampling rate was 50 kHz, and data were collected for 131 s for each measurement.

The second unit was a twin riser CFB, with two risers of 76 and 203 mm in diameter, sharing a 300-mm diameter common downcomer,[12] where experiments on CFB and HDCFB at high air velocities (over 5.0 m/s) were carried out. For all experiments, different solids circulation rates were maintained though adjusting the total solids inventory in the downcomer and the solids control valve. For CFB regime, the system operated at air velocities of 5.5 and 8.0 m/s and at the solids circulation rates of 50, 70, and 100 kg/(m^{2}s), whereas for HDCFB regime, it operated at air velocities of 5.0, 8.0, and 10 m/s and at solids circulation rates of 300, 400, and 550 kg/(m^{2}s). The solids holdup distributions were acquired with optical fiber probes at 11 equal area circles (r/R = 0.0, 0.16, 0.38, 0.5, 0.59, 0.67, 0.74, 0.81, 0.87, 0.92, and 0.98) at eight axial levels within the risers. Two samples were taken at each location, and the total sampling time was 60 s.

The particles used in these units were FCC catalyst with a Sauter mean diameter of 60–76 μm and a particle density of 1500–1780 kg/m^3. The relative humidity was kept between 70 and 80% by the addition of steam, which has been shown to effectively minimize the electrostatic effects.[24,25]

MCDPM

Parameters of moment consistency

The heterogeneous flow structures in a fluidized bed can be studied macroscopically and microscopically. Using measured solids holdup signals with the population N represented by Eq. 1, the overall flow structures may be characterized by signal moment estimations, such as mean solids holdup $\overline{\varepsilon}_s$, standard deviation σ, skewness S, and kurtosis K (Eqs. 2–5).

$$\{\varepsilon_i\},\ i \in N \tag{1}$$

$$\overline{\varepsilon_s} = \frac{1}{N}\sum_{i=1}^{N}\varepsilon_i \tag{2}$$

$$\sigma = \left[\frac{1}{N-1}\sum_{i=1}^{N}\left(\varepsilon_i - \overline{\varepsilon}_s\right)^2\right]^{1/2} \tag{3}$$

$$S = \frac{\sum_{i=1}^{N}\left(\varepsilon_i - \overline{\varepsilon}_s\right)^3}{(N-1)\sigma^3} \tag{4}$$

$$K = \frac{\sum_{i=1}^{N}\left(\varepsilon_i - \overline{\varepsilon}_s\right)^4}{(N-1)\sigma^4} \tag{5}$$

For an ideal completely segregated two-phase flow system, where exist only two values of solids holdups, namely, a high solids holdup representing that in the dense phase, ε_{sd}, and a low solids holdup representing that in the dilute phase, ε_{sb}, with f_d being the fraction of the dense phase, as represented by Eq. 6.

$$\{\varepsilon_{id} = \varepsilon_{sd}, \varepsilon_{ib} = \varepsilon_{sb}\}, \quad \text{id} \in N \ \text{ and } \ \text{ib} \in N \tag{6}$$

where the number of the elements in dense phase is $n\ (\varepsilon_{sd}) = f_d N$, and the number of the elements in dilute phase is $n\ (\varepsilon_{sb}) = (1 - f_d)N$.

For such an ideal case, Eqs. 2–5 can be simplified to Eqs. 7–10

$$\overline{\varepsilon}_s = f_d\varepsilon_{sd} + (1 - f_d)\varepsilon_{sb} \tag{7}$$

$$\sigma = \sqrt{(\varepsilon_{sd} - \overline{\varepsilon}_s)^2 f_d + (\varepsilon_{sb} - \overline{\varepsilon}_s)^2(1 - f_d)} \tag{8}$$

$$S = \frac{1}{\sigma^3}\left[(\varepsilon_{sd} - \overline{\varepsilon}_s)^3 f_d + (\varepsilon_{sb} - \overline{\varepsilon}_s)^3(1 - f_d)\right] \tag{9}$$

$$K = \frac{1}{\sigma^4}\left[(\varepsilon_{sd} - \overline{\varepsilon}_s)^4 f_d + (\varepsilon_{sb} - \overline{\varepsilon}_s)^4(1 - f_d)\right] \tag{10}$$

A typical data series (Series 1) for Eq. 1 from a CTFB is shown in Figure 2a, where a two-phase structure is clearly observed. A new series (Series 6, as represented by Eq. 6) may be generated as shown in Figure 2b to follow the trend of Series 1 as represented by Eq. 1. Comparing the two series shown in Figure 2, by adjusting the values ε_{sd} and ε_{sb} and their respective fractions f_d and f_b (= $1 - f_d$) in Series 6, it is possible to have at least three or four moments as calculated by Eqs. 7–10 to be equal to those obtained through Series 1 based on an experimental measurement. Therefore, the two series are considered to have the same sets of moments. Under such circumstances, it is hereby postulated that if the above two series (1 and 6) have the same sets of moments, the average values of the two phases and their respective fractions must be the same between the two series. In other words, ε_{sd}, ε_{sb}, and f_d ($f_b = 1 - f_d$) from Series 6 can be taken as (or at least be used to estimate) $\overline{\varepsilon}_{sd}$, $\overline{\varepsilon}_{sb}$, and f_d from Series 1 and then be used to analyze time series 1. Such an approach is proposed here as a MCDPM.

For analysis, the four moments will first be calculated from the experimental series Eq. 1. Then, the four moment values will be applied in Eqs. 7–10 to back calculate the three key parameters ε_{sd}, ε_{sb}, and f_d. However, as there are three unknowns and four equations, it is necessary to make a proper combination of three equations out of the four equations (Eqs. 7–10) to produce the most pertinent results. As the two most important characteristics of the two-phase flow, the mean and standard deviation should remain consistent between the two series and, therefore, always be included in the calculation. The next moment equation to be included can be chosen from the skewness and the kurtosis, each referring to equal important properties of a series, depending on what parameters are being examined. Thus, there are two combinations or two methods, Eqs. 7–9 or Eqs. 7, 8, and 10, to process the data into the parameters of the dense and dilute phases. As a first approach, the combination of Eqs. 7–9, including skewness, can be rearranged in the following explicit expressions (Eqs. 11–13), with detailed derivations given in Qi.[10]

Method 1.

$$f_d = \frac{1}{2}\left(1 - S\sqrt{\frac{1}{4 + S^2}}\right) \tag{11}$$

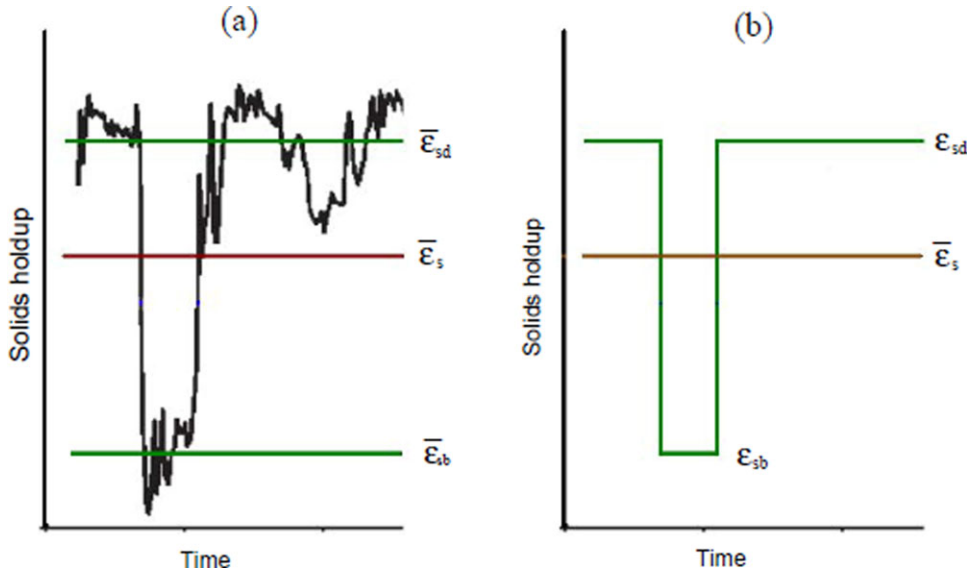

Figure 2. Segment of (a) measured solids holdup signals of CTFB vs.; (b) the solids holdup signals from the corresponding ideal two-phase flow.

[Color figure can be viewed in the online issue, which is available at wileyonlinelibrary.com.]

$$\varepsilon_{sd} = \bar{\varepsilon}_s + \frac{\sigma}{2}\left[\sqrt{4+S^2}+S\right] \tag{12}$$

$$\varepsilon_{sb} = \bar{\varepsilon}_s - \frac{\sigma}{2}\left[\sqrt{4+S^2}-S\right] \tag{13}$$

Similarly, a second approach is to include kurtosis, using the combination of Eqs. 7, 8, and 10, leading to the following explicit expressions (Eqs. 14–16), with detailed derivation shown in Qi.[10]

Method 2.

$$f_d = \frac{1}{2}\left(1 \pm \sqrt{\frac{K-1}{3+K}}\right) \tag{14}$$

$$\bar{\varepsilon}_{sd} = \bar{\varepsilon}_s + \frac{\sigma}{2}\left(\sqrt{K+3} \mp \sqrt{K-1}\right) \tag{15}$$

$$\bar{\varepsilon}_{sb} = \bar{\varepsilon}_s - \frac{\sigma}{2}\left(\sqrt{K+3} \pm \sqrt{K-1}\right) \tag{16}$$

To evaluate the proper applicable conditions of these two methods for the desirable results, the relative errors of the other moment, not included in the data processing through either M1 or M2, reduced to the same dimension as the experimental data, can be estimated by Eqs. 17 and 18. When using Method 1 (M1), the relative error on kurtosis between the Series 1 and 6 is

$$E_K = \frac{\left|K^{1/4} - K_{th}^{1/4}\right|}{K^{1/4}} \tag{17}$$

Similarly, the relative moment error on skewness with Method 2 (M2) is

$$E_S = \frac{\left|S^{1/3} - S_{th}^{1/3}\right|}{S^{1/3}} \tag{18}$$

where S_{th} and K_{th}, the theoretical skewness and kurtosis, are calculated using Eqs. 9 and 10, respectively, from the known values of ε_{sd}, ε_{sb}, f_d, and $\bar{\varepsilon}_s$, and S and K, the actual skewness and kurtosis, are obtained from Eqs. 4 and 5, respectively.

For a given solids holdup distribution, relative large moment errors may occur due to the skewness or kurtosis not being included, depending on what method is selected. Figure 3 displays the relative errors of M1 and M2 for solids holdup distributions at 11 radial positions at four elevations under 56 experimental conditions of high-density gas–solids flow. The results demonstrate that M1 predicts the solids holdups of the dense and dilute phases and the dense phase volume fraction with small moment errors in kurtosis at small absolute skewness values, and large kurtosis error happens at the large absolute skewness values (Figure 3a). On the other hand, M2 computes the parameters with small moment errors in skewness at large kurtosis values, and the error in skewness increases as the value of kurtosis decreases toward zero. The results demonstrate that the selection for most pertinent results between M1 and M2 might be made through evaluating the magnitudes of the skewness or kurtosis, corresponding to the minimum moment error defined by Eqs. 17 and 18.

Plotting all skewness and kurtosis calculated through Eqs. 4 and 5 for all experimental data listed in Table 1 gives rise to a parabolic strap on the *K*–*S* plane, as shown in Figure 4. Checking the values of the errors in skewness, E_S, and kurtosis, E_K, as computed by Eqs. 17 and 18 and plotted in Figure 3, corresponding to the *S*–*K* values plotted in Figure 4, the method that results in lesser errors is marked out in Figure 4. Interestingly, the regimes where M2 is applicable are clearly separated from that of M1, with M2 in the two tailing straps and M1 in the nose region. With such a clear mapping, the selection of the methods of MCDPM for a specific solids holdup distribution is now made easier, as it can be determined directly using the skewness or kurtosis values as expressed in Eq. 19.

$$\text{M1 for } |S|<1.5 \text{ or } K<4.5 \tag{19a}$$

and

$$\text{M2 for } |S| > 1.5 \text{ or } K > 4.5 \tag{19b}$$

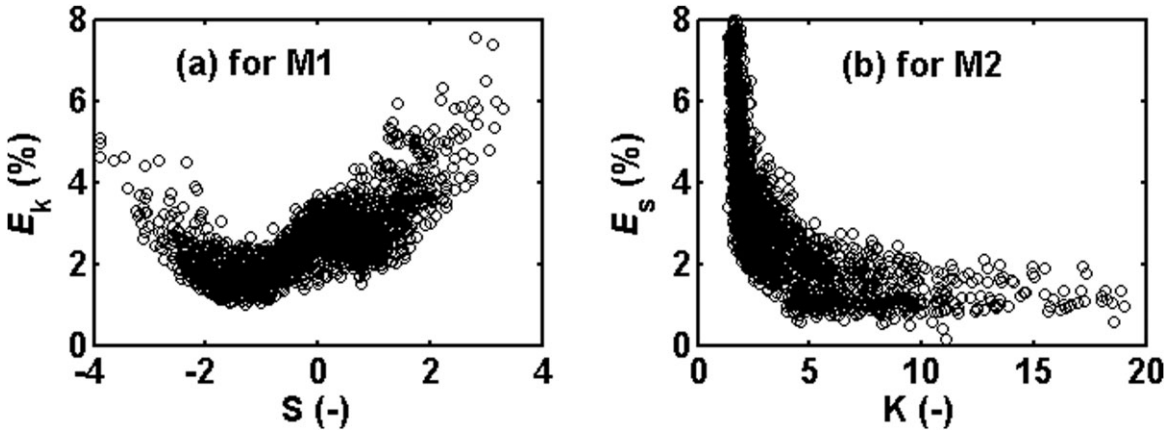

Figure 3. Relative moment errors of MCDPM with respect to (a) skewness or (b) kurtosis of local solids holdup signals.

Dividing dense and dilute phases

Dividing the dense and dilute phases from a solids holdup time series requires finding a division value, a special solids holdup, to identify the transition between the two phases. Using the dense phase fraction, f_d, a number n can be obtained by Eq. 20, from a solids holdup time series with population N, for example, Series 1 from Eq. 1.

$$n = f_d N \tag{20}$$

If the time series is sorted in a descending order, the nth solids holdup value in the sorted series, ε_s (n), will be the division value. Thus, the subset of the solids holdup numbered up to n in the sorted series includes all members of the dense phase, and the rest includes all members of the dilute phase in the measured time series. As a result, the dense and dilute phases can be divided from the measured time series using the determined value ε_s (n).

Considering that time series 1 represents a series of solids holdup values over time at a given location inside the fluidized bed, the dense phase time fraction in the time series actually also represents the volume fraction of the dense phase at that given location. As well, the average dense and dilute phase holdups in the time series would represent the solids holdups of the dense and dilute phases at the given location.

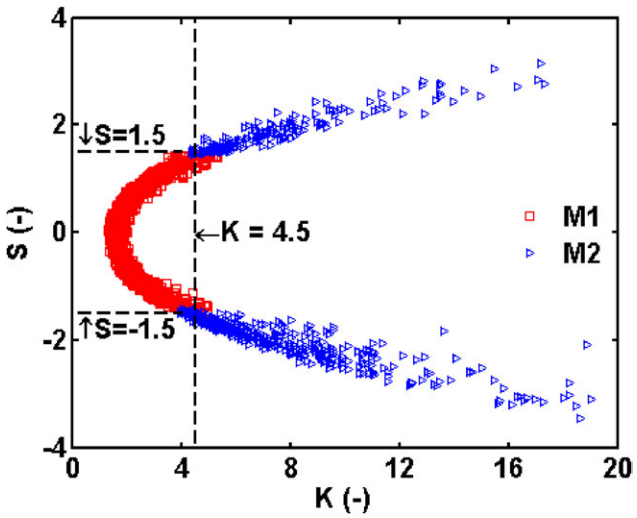

Figure 4. Relationship of skewness and kurtosis for all solids holdup signals.

[Color figure can be viewed in the online issue, which is available at wileyonlinelibrary.com.]

Results and Discussion

As discussed in the "Introduction" section, fluidized beds experience five major different operating regimes with increasing gas velocity, the bubbling fluidization, the turbulent fluidization, the circulating turbulent fluidization, the high-density circulating fluidization, and the low-density circulating fluidization. Studies on those fluidized beds and their flow characteristics have been extensively reported, as partially reviewed in the "Introduction" section and more thoroughly reviewed by several researchers.[1,5,6,14,26] Having said that, more systematic studies to understand the underlining characteristics over the various flow regimes are still lacking, mostly because the effective tools that can quantify such characteristics over the all the various fluidization regimes are not available. With the new MCDPM moment analysis method developed here, we can obtain three key flow parameters, the solids holdup inside the dense phase, the solids holdup inside the dilute phase, and the dense phase fraction (dilute phase fraction is, therefore, known as those two add to unity), over a wide range of operating conditions encompassing all key fluidization flow regimes, and more importantly at almost unlimited axial and radial locations in those fluidized beds, from simple time series measurements for local solids holdups. With such ample availability of data, although still limited to three parameters, key characteristics of the above-mentioned five regimes can be readily quantified and compared, to provide more insights to fluidization.

Flow structure across regimes

Figures 5–7 provide the profiles of the solids holdups of the dense and dilute phases and the dense phase volume fraction of BFB, TFB, CTFB, HDCFB, and CFB obtained by MCDPM, whose operating conditions are listed in Table 2. The profiles demonstrate that different fluidization regimes have different flow structures. For the dilute phase, BFB, TFB, and CTFB share similar solids holdup profiles, which do not change appreciably (around 0.06) in the core region but increase quickly toward the wall to up to about 0.20. Further increasing the air velocity to enter HDCFB and CFB regimes, the profiles of the dilute phase solids holdups (the

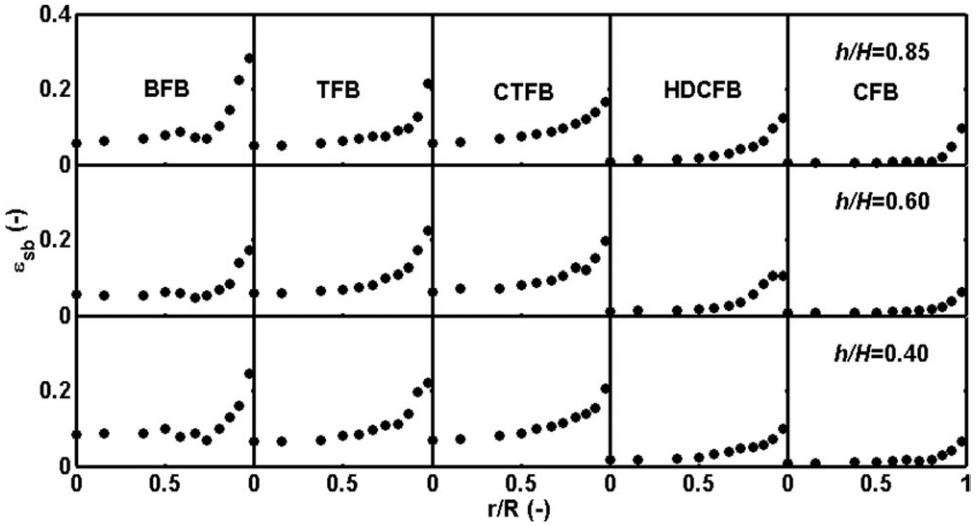

Figure 5. Radial solids holdup profiles of the dilute phase of BFB (u_g = 0.53 m/s), TFB (u_g = 1.6 m/s), CTFB [u_g = 2.57 m/s, G_s = 234 kg/(m^{2}s)], HDCFB [u_g = 8 m/s, G_s = 550 kg/(m^{2}s)], and CFB [u_g = 8 m/s, G_s = 100 kg/(m^{2}s)]; data for HDCFB and CFB from Yan and Zhu.[12]

solids holdup inside the dilute phase), although still in parabolic shape, are seen to have much smaller magnitudes than those in BFB, TFB, and CTFB, both in the center and at the wall (Figure 5). However, the profile of the dilute phase solids holdup for CTFB is seen to have a more gradual increase toward the wall than all other four regimes and a lower value at the wall than BFB and TFB. For the dense phase (Figure 6), BFB, TFB, and CTFB have same uniform profiles of the dense phase solids holdups (the solids holdup inside the dense phase) across the bed except that CTFB has a slight but steady increase from the center toward the wall, corresponding to the values from 0.45 at the center to 0.50 at the wall. Much different from the uniform radial distribution of BFB, TFB, and CTFB, the dense phase solids holdup profiles of HDCFB and CFB are characterized by the typical core-annular structure, with the solids holdups in the core region of HDCFB and CFB much less than those of BFB, TFB, and CTFB and increasing quickly in the annular region. Despite similarities between HDCFB and CFB profiles, significant differences are observed in the magnitudes of the solids holdups of the dense phase, with HDCFB varying from ~0.05 to ~0.5, whereas CFB from ~0.03 to ~0.20. Further examining the dilute phase profiles for HDCFB and CFB can also reveal some differences between the two regimes, although on a much smaller scale, with HDCFB varying from ~0.01 to ~0.15 whereas CFB from ~0.01 to ~0.10.

Compared to the solids holdup profiles of the dense and dilute phases, the profiles of the dense phase volume fraction vary differently across the fluidization regimes, as shown in Figure 7. BFB regime is dominated by dense phase with dense phase volume fractions of 0.6 or greater throughout the bed, whereas HDCFB and CFB regimes are clearly dominated by dilute phase with dense phase volume fractions mostly lower than 0.2 except near the wall area. Unlike the phase holdup profiles for both dense and dilute phases, the radial profiles of the dense phase volume fraction for both TFB

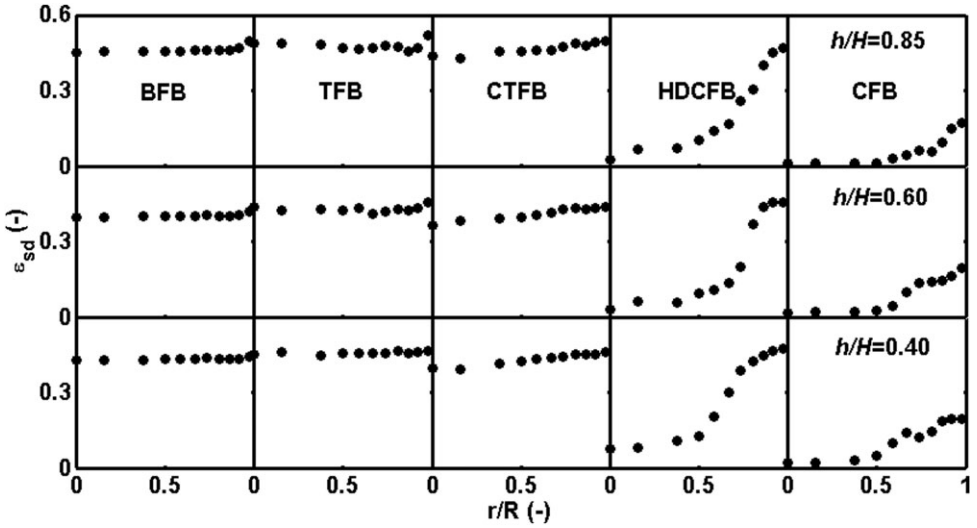

Figure 6. Solids holdup profiles of dense phase of BFB (u_g = 0.53 m/s), TFB (u_g = 1.6 m/s), CTFB [u_g = 2.57 m/s, G_s = 234 kg/(m^{2}s)], HDCFB [u_g = 8 m/s, G_s = 550 kg/(m^{2}s)], and CFB [u_g = 8 m/s, G_s = 100 kg/(m^{2}s)]; data for HDCFB and CFB from Yan and Zhu.[12]

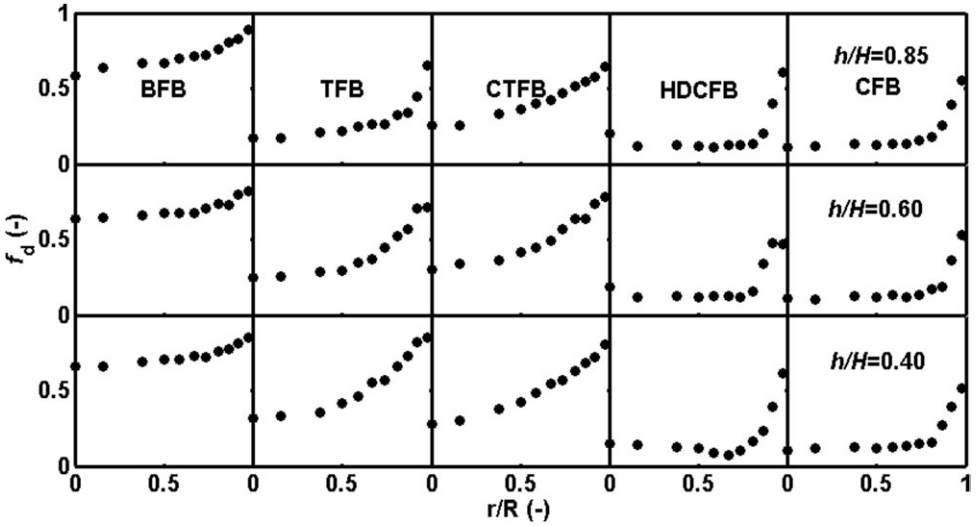

Figure 7. Profiles of dense phase fraction of BFB (u_g = 0.53 m/s), TFB (u_g = 1.6 m/s), CTFB [u_g = 2.57 m/s, G_s = 234 kg/(m^{2}s)], HDCFB [u_g = 8 m/s, G_s = 550 kg/(m^{2}s)], and CFB [u_g = 8 m/s, G_s = 100 kg/(m^{2}s)]; data for HDCFB and CFB from Yan and Zhu.[12]

and CTFB are completely different from that of BFB, increasing steadily from the center to the wall. Additionally, the volume fraction profiles for TFB and CTFB appear to be nearly indistinguishable, suggesting that CTFB is clearly a turbulent fluidization regime although significant external solids circulation has been introduced. Likewise, the volume fraction profiles for CFB and HDCFB are also extremely similar, both having typical clear core-annulus structure, suggesting a possible common root for those two regimes.

Flow regime transition and similarities

Through a comprehensive examination of all results shown in Figures 5–7, the mechanism of the regime transitions through the various fluidization regimes can be revealed. The overall average values of ε_{sb}, ε_{sd}, and f_d are plotted against the fluidization regimes in Figure 8, from low-velocity fluidization regimes (BFB, TFB, and CTFB) to high-velocity fluidization regimes (HDCFB and CFB). For the dense phase, its average values stay relatively constant in the low-velocity regimes but decreases with increasing gas velocity in the high-velocity regimes. For the dilute phase, the situation is similar, although somewhat less significant than the dense phase. On the other hand, the dense phase fraction, f_d, decreases dramatically with increasing velocity, through bubbling, turbulent (TFB and CTFB), and high-velocity regimes (HDCFB and CFB). From those trends, it can be postulated that from low velocity up, the regime transition starts with the increase of the dilute phase fraction, while the magnitudes of both solids holdups in the dense and dilute phases remain constant, within the three low-velocity fluidization regimes. In other words, within low-velocity regimes, the values of the solids holdups in both the dilute and the dense phases do not change much, but the relative volume (fraction) of the dense phase shrinks with increasing velocity. The most significant change in the flow structure, that is, regime transition, happens between CTFB and HDCFB, where the dense phase holdups, as well as but to a smaller extent the dilute phase holdups, begin to decrease, while the dense phase fraction continues to decrease, with increasing gas velocity. Therefore, one may say that this transition has a more profound change in the flow structure, or the transition between CTFB and HDCFB represents a more dramatic regime transition than those within each one of the low-velocity and high-velocity

Table 2. RNI and Average Value for the Dilute and Dense Phase Solids Holdups and the Dense Phase Volume Fraction

	BFB	TFB	CTFB	HDCFB	CFB
Dense phase fraction					
Average Value	0.72	0.43	0.49	0.21	0.20
RNI	0.02	0.03	0.04	0.60	0.31
Dense phase holdups					
Average Value	0.43	0.45	0.44	0.24	0.08
RNI	0.20	0.20	0.21	0.24	0.17
Dilute phase holdups					
Average Value	0.10	0.10	0.11	0.04	0.02
RNI	0.13	0.24	0.27	0.35	0.34

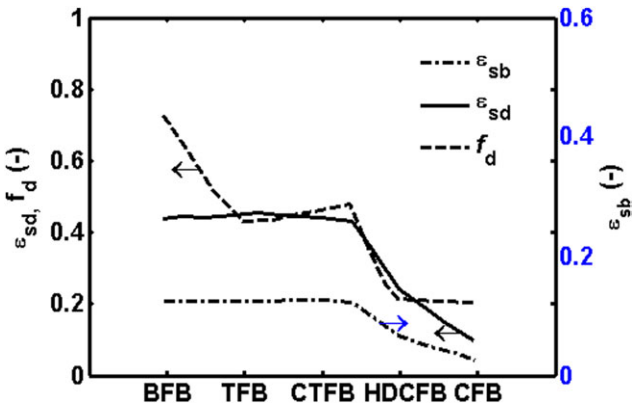

Figure 8. Variation of average values of ε_{sb}, ε_{sd}, and f_d across the fluidization regimes, BFB (u_g = 0.53 m/s), TFB (u_g = 1.6 m/s), CTFB [u_g = 2.57 m/s, G_s = 234 kg/(m^{2}s)], HDCFB [u_g = 8 m/s, G_s = 550 kg/(m^{2}s)], and CFB [u_g = 8 m/s, G_s = 100 kg/(m^{2}s)]; data for HDCFB and CFB from Yan and Zhu.[12]

[Color figure can be viewed in the online issue, which is available at wileyonlinelibrary.com.]

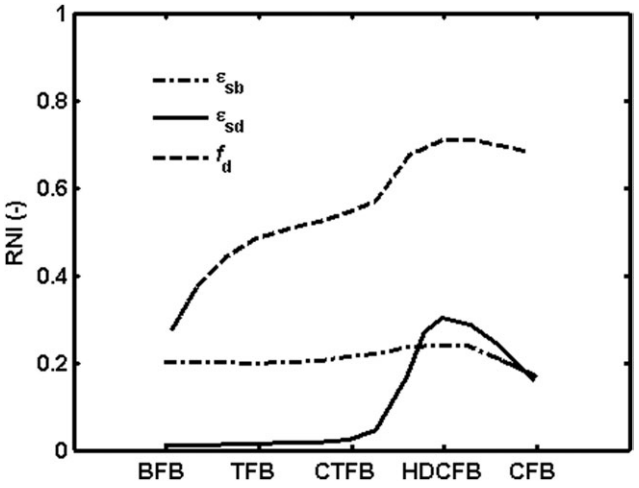

Figure 9. RNI of ε_{sb}, ε_{sd}, and f_d at h/H =0.60 for five fluidization regimes, BFB (u_g = 0.53 m/s), TFB (u_g = 1.6 m/s), CTFB [u_g = 2.57 m/s, G_s = 234 kg/(m^{2}s)], HDCFB [u_g = 8 m/s, G_s = 550 kg/(m^{2}s)], and CFB [u_g = 8 m/s, G_s = 100 kg/(m^{2}s)]; data for HDCFB and CFB from Yan and Zhu.[12]

regimes. In the high-velocity regimes, the phase holdups begin to have more changes, while the phase fractions experience little change, and the transition between HDCFB and CFB is more signified by values of the phase holdups rather than their relative phase fractions.

Further examining Figure 8, one should be able to notice that TFB and CTFB have almost the same flow structures in terms of solids holdup and, therefore, may be considered being operated under very similar regimes. Noting that the particle velocity in CTFB would not be zero given the external solids recirculation, the difference between the TFB and CTFB regimes would be mostly on that CTFB has a net particle upflow.[8] Such net upward solids flow also seems to yield a slightly more obvious variation in radial solids holdup in the CTFB regime than in the TFB regime. On the contrary, the differences between the flow structures in the HDCFB and CFB are more significant than those between TFB and CTFB. This transition (between HDCFB and CFB) may be similar in magnitude as the transition between BFB and TFB but with the changes both in "quantity" (the relative division of the phases) and "quality" (the phase holdup values). On the other hand, the transition between the low-velocity and high-velocity regime groups, as represented by the transition between CTFB and HDCFB, is more on the change in the phase holdup values ("quality") rather than the division of the two phases ("quantity").

Such a change of first in the reduction of dense phase fraction and then the reduction of the solids holdup values of the two phases, in the regime transitions with increasing gas velocity and as discussed above with respect to Figure 8, can also be observed with increasing radial distances from the center toward the wall. As reported by Zhu and Zhu,[27] regime transition can happen gradually with respect to the locations inside a fluidized bed. Careful analyses over Figures 5–7 suggest that the regime transition starts from the center of the bed and then propagates toward the wall. For example, Figure 7 shows that the reduction in dense phase fraction first starts from the bed center with increasing gas velocity, whereas Figure 6 shows little change in dense phase holdups in the low-velocity regimes. When the dense phase holdup does begin to change, its change also starts from the center, gradually toward the wall, as shown by the radial profiles of the dense phase holdup in HDCFB and CFB in Figure 6. For the dilute phase solids holdup shown in Figure 5, there is also a clear trend that reduction in phase holdups starts from the center toward the wall and only propagates to the wall region under the high-velocity regimes. Experimentally, the above postulation has been verified by the results of Qi et al.[9]

To further evaluate transitions among the five fluidization regimes, the radial nonuniformity indices (RNIs) for ε_{sb}, ε_{sd}, and f_d, as proposed by Zhu and Manyele,[28] are plotted in Figure 9 for the various regimes. This radial nonuniformity index has a value between 0 and 1 and represents the relative uniformity in the radial profiles with 0 indicating a flat and uniform profile. For example, for radial solids holdup distribution, the RNI is obtained by dividing the standard deviation of those holdup data in the radial profile by the maximum possible standard deviation of the most nonuniform (least uniform) radial distribution of solids concentration under the same cross-sectional average solids concentration.[28] As such, the RNI values may be used to illustrate the flow development in the radial direction for the various regimes. Within the low-velocity fluidization regimes, RNI(ε_{sb}) and RNI(ε_{sd}) remain relatively constant, suggesting more uniform fluidization and less variation in special regime transition. Into the high-velocity regimes, RNI(ε_{sb}) and RNI(ε_{sd}) both have an obvious increase in HDCFB and then drop off into CFB, with the effect being very dramatic for the dense phase. RNI(f_d) shows a similar trend but has a clear dip for CFB, suggesting that the division between the dense and dilute phases is more uniform across the bed than TFB/CTFB. The above-mentioned phenomena echo at least partially the trends shown in Figure 8 and certainly illustrate the differences and transitions between the various fluidization regimes.

Flow regime differences and similarities

From the above analyses, it can be seen that the differences between each pair of neighboring regimes and therefore the transition in between are not always the same and as a matter of fact can be dramatically different. Table 2 summarizes the values of the averages and RNIs of ε_{sb}, ε_{sd}, and f_d as used in Figures 8 and 9. Following the same trend of Figures 8 and 9, one can see that these parameters do not change much in the low-velocity regimes but have a large jump crossing into HDCFB regime, and then "moderate" to a smaller change going into CFB regime. The extent of the above changes may be used to explore similarities among the various regimes.

As discussed above, TFB and CTFB have almost the same characteristics with minor differences, so that they may be considered as a single regime. Between TFB (as well as CTFB) and BFB, the only difference seems to be the relative fractions of the dense and dilute phases, so that the difference is small and quantitative. In general, BFB is characterized by large bubbles going through the central areas of the bed, whereas TFB by smaller voids more uniformly distributed across the bed. In other words, the transition is more on the changes in the size of the voids, while the dense phase remains the continuous phase. Therefore, TFB (including CTFB) still shares many similarities with BFB and should

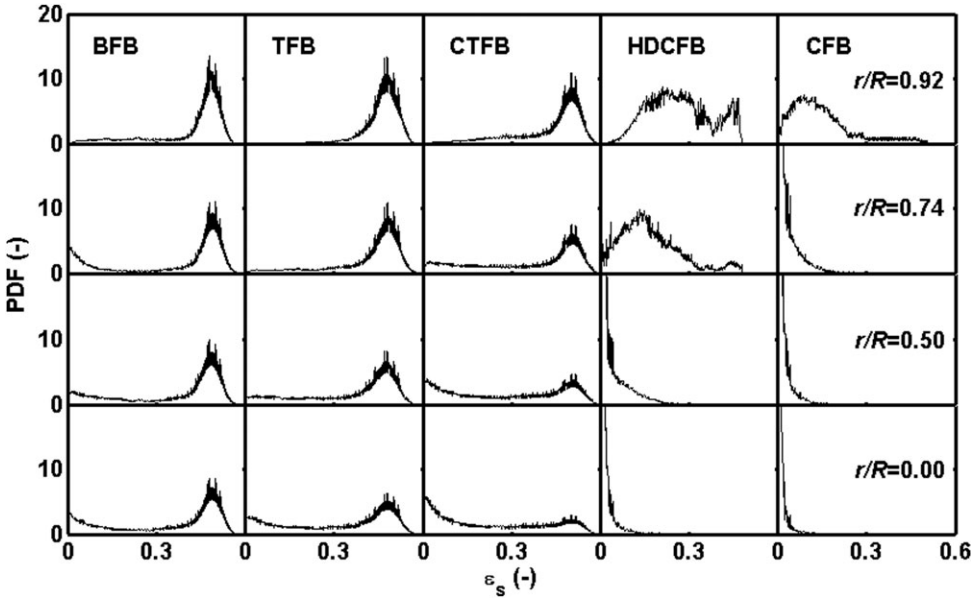

Figure 10. PDF profiles of BFB (u_g = 0.53 m/s), TFB (u_g = 1.6 m/s), CTFB [u_g = 2.57 m/s, G_s = 234 kg/(m^{2}s)], HDCFB [u_g = 8 m/s, G_s = 550 kg/(m^{2}s)], and CFB [u_g = 8 m/s, G_s = 100 kg/(m^{2}s)], corresponding to the data at h/H = 0.60 in Figures 11 and 12; data for HDCFB and CFB from Yan and Zhu.[12]

be still grouped with BFB and considered a low-velocity fluidization, rather than high-velocity fluidization. Entering into the high-velocity regimes, the flow is more characterized with a continuous dilute phase and dispersed dense phase aggregates. Such a dramatic change is clearly exhibited in Table 2 on all the parameters presented, reflecting the fact that this is a more fundamental change (regime transition) in the flow structure, where the two phases inverse their role as the dominant phase. Furthering into the CFB regime with increasing gas velocity, the relative changes in the parameters become smaller again, indicating a smaller change or a milder transition from HDCFB. However, the relative changes between HDCFB and CFB are still larger than those between BFB and TFB/CTFB.

From the above discussion and based on a wide span of the gas–solids multiphase flow systems in all fluidized beds, one can conclude:

1. TFB and CTFB may be considered a similar regime, possibly representing a transition between BFB and high-velocity fluidization.[10]

2. The differences between TFB/CTFB and BFB are relatively small.

3. CTFB, although having net external solids circulation like HDCFB/CFB, is essentially still a turbulent regime, similar to TFB.

4. The transition between TFB/CTFB and HDCFB is much more significant than any other transitions.

5. There is a clear difference between HDCFB and CFB, and such difference is larger than the difference between BFB and TFB.

Microscopic flow structure analyses

The differences between BFB, TFB, CTFB, HDCFB, and CFB regimes can be further studied by the natures of PDF of the solids holdups and moment features, such as skewness and kurtosis, as shown in Figures 10–12. The results demonstrate that the fluidization regimes can be classified into two groups: flow dominated by high solids holdup peak and flow dominated by the dilute phase peak (Figure 10), corresponding to the low-velocity and high-velocity fluidization regime groups discussed earlier. In the first group, BFB, TFB, and CTFB have a clear peak in their PDF graphs around the dense phase solids holdup and a more scattered dilute phase distribution. The dense phase peak also increases from the center toward the wall, whereas the magnitude of the dilute phase reduces from the center to the wall, implying much denser phase dominating toward the wall. In the second group, HDCFB and CFB only display a dilute phase peak on the left side in their PDF graphs, implying dilute phase dominating. From the center to the wall, the dilute phase peak widens and shifts right, responding to the weakened dilute phase structure. The lack of high-density peak for HDCFB and CFB regimes echoes the low-density fraction as shown in Figure 8.

The differences between the fluidization regimes displayed by PDF can be exhibited through the skewness and kurtosis features of the solids holdups, as shown in Figures 11 and 12. Typically, skewness is a measure of the lack of symmetry in the PDF of the solids holdup signals around the mean value and reflects the predominance between the dense and dilute phases in the gas–solid phase flow, negative skewness reflecting dense phase dominating flow and positive skewness reflecting dilute phase dominating flow. The negative skewness in BFB and most of TFB and CTFB confirms the dense phase dominated flow, whereas the high skewness in HDCFB and CFB confirms the dilute phase dominated flow. For CTFB and to a lesser extent also for TFB, the skewness is close to zero in the center, suggesting a beginning of the transition of the flow from dense phase dominating to dilute phase dominating. On the other hand, kurtosis is a measure of the peakedness of the PDF and quantifies the magnitude of the variation of solids holdup distribution of the dispersive phase (bubbles in BFB and clusters in CFB). Therefore, the long and sharp tails in the PDF in Figure 10 lead to higher kurtosis values, corresponding to the solids distribution in the core region of HDCFB and CFB and in the wall region of BFB, TFB, and CTFB. On the other hand, a widen

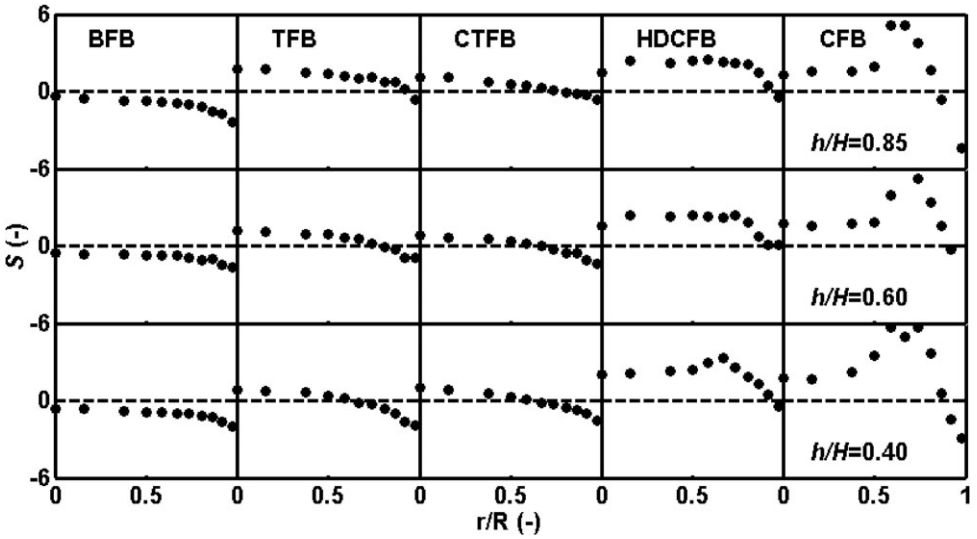

Figure 11. Radial skewness profiles for BFB (u_g = 0.53 m/s), TFB (u_g = 1.6 m/s), CTFB [u_g = 2.57 m/s, G_s = 234 kg/(m^{2}s)], HDCFB [u_g = 8 m/s, G_s = 550 kg/(m^{2}s)], and CFB [u_g = 8 m/s, G_s = 100 kg/(m^{2}s)]; data for HDCFB and CFB from Yan and Zhu.[12]

distribution on the PDF in Figure 10 corresponds to lower kurtosis values, representing the solids holdup distributions in the core region of BFB, TFB, and CTFB and in the wall region of HDCFB and CFB.

Underlining mechanisms flow characteristics across fluidization regimes

When a gas–solid bed starts to fluidize at minimum fluidization velocity, the entire bed is in the dense phase condition. With increasing gas velocity, dilute phase appears and the dilute phase fraction also increases with further increasing gas velocity. This is due to particle aggregation and leads to nonuniformity in gas and solids flow distribution, both in terms of phase holdups and phase flow, inside the fluidized bed.[29] Although making many things less ideal, it is such nonuniformity that provides the main feature of gas–solid fluidized bed, allowing a gas–solid fluidized bed to operate at high gas velocities well beyond the particle terminal velocity and, therefore, significantly increases the process capacity of fluidized bed reactors.

Results obtained in this studies as reported above have allowed us to track the gradual evolvements of the two phases through the various fluidized bed systems, with increasing gas velocity. Initially, dilute phase appears as soon as extra gas is added after minimum fluidization velocity for Geldart Group B particles or soon after at minimum bubbling velocity for Geldart Group A particles. Our study shows that with such increase in the dilute phase fraction in the bed (or the decrease in the dense phase fraction, as plotted in Figures 7 and 8), the solids holdups inside both the dilute and the dense phases do not change appreciably over an extended region covering bubbling and (circulating) turbulent regimes, with increasing gas velocity. Considering the fundamental forces that govern the gas–solid flow inside an ideal fluidized bed, the particles are dragged upward by the gas flow (drag force) and downward by the gravitational

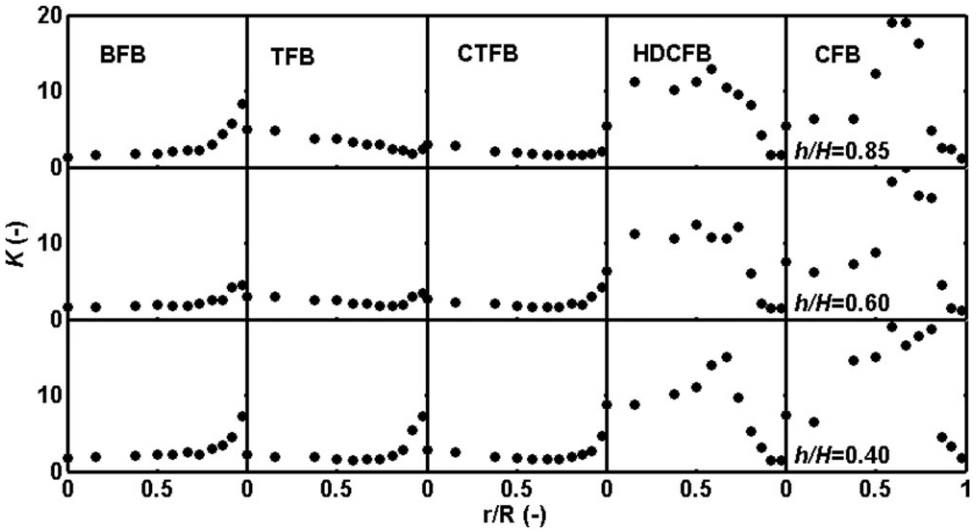

Figure 12. Radial kurtosis profiles for BFB (u_g = 0.53 m/s), TFB (u_g = 1.6 m/s), CTFB [u_g = 2.57 m/s, G_s = 234 kg/(m^{2}s)], HDCFB [u_g = 8 m/s, G_s = 550 kg/(m^{2}s)], and CFB [u_g = 8 m/s, G_s = 100 kg/(m^{2}s)]; data for HDCFB and CFB from Yan and Zhu.[12]

force (with the buoyancy force neglected). When drag and gravity reach equilibrium, the particles are successfully suspended, fluidized. However, as pointed out by the bifurcation theory for two-phase flow,[30,31] with multiple particles inside the gas–solid fluidized bed system, the most stable operation is likely to be achieved with flow bifurcation, that part of the fluidized bed would be much more dilute than the rest of the bed, allowing the easy passage of excess gas, while retaining most particles in the dense phase, so that to minimize the overall energy consumption.[32]

Thus, the formation of bubbles is the result of the bifurcation and the solids holdups of the dilute and dense phases that would achieve stable operation are also dictated by the bifurcation and/or energy minimization. As a result, further increasing gas velocity from bubbling bed into the TFB would only increase the fraction of the dilute phase but not the solids holdups of the dilute and dense phases. This is clearly shown in Figure 8 where the solids holdups in both dilute and dense phases remain constant over BFB, TFB, and CTFB. Those fluidized beds are termed as low-velocity fluidized bed. With yet further increasing the gas velocity, the overall fluidized bed becomes so dilute that the flow mechanism underlining the gas–solid flow changes. Essentially, the dense phase begins to loose its dominance and gives right of the continuous phase to the dilute phase. Particle aggregation, while still existing, also changes its form to particle clusters, in which size, and possibly also density, decreases with the increase of gas velocity. In those high-velocity fluidized bed, the solids holdups in both dense and dilute phases continue to decrease with increasing gas velocity, as also clearly shown in Figure 8. It has been reported in our earlier study[9] that the gas–solids flow inside low-velocity fluidization systems is dominated by particle–particle interaction, so that the solids holdups inside the two phases in BFB, TFB, and CTFB are not affected much by the gas velocity. It may be further extended that the gas–solids flow inside high-velocity fluidization systems is more dominated by gas–particle interaction, so that the solids holdups inside the two phases in HDCFB and CFB change drastically with increasing gas velocity.

As only FCC, Geldart Group A particle, was used in this study, some of the above discussion may not apply to other types of Geldart particles. For example, the two-phase behavior for larger Geldart Group B particles are much stronger than those of Group A particles, so that even the existence of the transition regime, the turbulent fluidization regime, is still a question.[33]

Significance of MCDPM

MCDPM includes moment feature analysis (mean, standard deviation, skewness, and kurtosis), parameter estimation and phase division of the flow structure in multiphase flow systems. Compared to other investigation methods on flow structures in gas–solid systems, MCDPM is capable of directly estimating solids holdups of the dense and dilute phases and the dense phase volume fraction from the measured solids holdup series, without additional information. With calculated ε_{sd}, ε_{sb}, and f_d, from measurements at various axial and radial locations, one can easily study the detailed two-phase flow structure in many fluidized beds and other multiphase conditions. In particular, flow regime classification and characterization are made possible over a wider range of conditions.

Conclusions

Experiments with FCC particles were carried out in two fluidized beds under five different fluidization regimes, BFB, TFB, CTFB, HDCFB, and CFB. Solids holdup signals were obtained with optical fiber probes at eleven radial positions at four elevations. The moments (mean, standard deviation, skewness, and kurtosis) from the experimentally measured solids holdup signals were compared with those of equivalent ideal two-phase flow systems, and a MCDPM was proposed to estimate the solids holdups and volume fractions of the dense and dilute phases at each measured location. These key parameters and their radial and axial distributions were used to study the detailed flow structures inside the various fluidized beds and the regime transitions among them. The results showed great similarities between the TFB and CTFB but less similarities between the HDCBF and the CFB, with a more significant regime transition from TFB/CTFB to HDCFB. In the low-velocity regimes of BFB, TFB, and CTFB, increasing gas velocity leads only to the decreasing of dense phase fraction but not the average dilute and dense phase holdups, whereas in the high-velocity regimes from HDCFB to CFB, it is the solids holdups of the dense phase that undergoes the most change. From the low-velocity to the high-velocity regimes, both the solids holdup and the fraction of the dense phase experience a drastic decrease, suggesting that this transition has a more profound change in the flow structure and further suggesting that CTFB is in reality still a TFB, although external solids recirculation has been imposed. Across the bed, the regime transition starts from the center of the bed and then propagates toward the wall.

Acknowledgments

The authors are grateful to the Natural Sciences and Engineering Research Council of Canada for supporting this work.

Notation

D = bed diameter, m
E_K = relative kurtosis error
E_S = relative skewness error
f_d = volume fraction of dense phase
G_s = circulation rates, kg/(m^{2}s)
K = kurtosis of local solids holdup fluctuations
K_{th} = theoretical kurtosis value
N = sampling population
n = the population number of the subset of the solids holdup within dense phase
r = radial position, m
R = radius of the column, m
S = skewness of local solids holdup fluctuations
S_{th} = theoretical skewness value
u_g = superficial air velocity, m/s
v_p = instantaneous particle velocity, m/s
V_p = particle velocity, m/s
Z = elevation from the air distributor, m

Greek letters

ε = instantaneous solids holdup
$\bar{\varepsilon}_s$ = local time-averaged solids holdup
ε_{sb} = local time-averaged solids holdup of dilute phase
ε_{sd} = local time-averaged solids holdup of dense phase
ρ_p = particle density, kg/m^3
σ = standard deviation of local solids holdup fluctuations

Subscripts

c = phase
b = dilute phase
g = gas
p = particle
s = solids

Literature Cited

1. Grace JR, Avidan AA, Knowlton TN. *Circulating Fluidized Bed*. London: Blackie Academic and Professional (Chapman & Hall), 1997.
2. Zhu J. Circulating turbulent fluidization—a new fluidization regime or just a transitional phenomenon. *Particuology*. 2010;8:640–644.
3. Kehoe PWK, Davidson JF. *Continuously slugging fluidized beds*, In: *Chemeca'70, Institution of Chemical Engineers Symposium Series*, Vol. 33. Australia: Butterworths, 1970:97–116.
4. Zhu J, Cheng Y. *Fluidized-bed reactors and applications*. In: Crowe C, editor. *Multiphase Flow Handbook*. New York: CRC Press, 2005:5.55–5.93.
5. Zhu J, Bi HT. Distinctions between low density and high density circulating fluidized beds. *Can J Chem Eng*. 1995;73:644–649.
6. Grace JR. High-velocity fluidized bed reactors. *Chem Eng Sci*. 1990;45:1953–1966.
7. Zhu H, Zhu J. Gas–solids flow structures in a novel circulating-turbulent fluidized bed. *AIChE J*. 2008;54:1213–1223.
8. Zhu H. Zhu J. Comparative study of flow structures in a circulating-turbulent fluidized bed. *Chem Eng Sci*. 2008;63:2920–2927.
9. Qi X, Zhu H, Zhu J. Demarcation of a new circulating turbulent fluidization regime. *AIChE J*. 2009;55:594–611.
10. Qi M. Hydrodynamics and micro flow structure of gas–solid circulating turbulent fluidized beds, Ph.D. dissertation. London, Ontario: Western University, 2012.
11. Bi HT, Su P. Local phase holdups in gas–solids fluidization and transport. *AIChE J*. 2001;47:2025–2031.
12. Yan A, Zhu J. Scale-up effect of riser reactors (1): axial and radial solids concentration distribution and flow development. *Ind Eng Chem Res*. 2004;43:5810–5819.
13. Abbasi M, Sotudeh-Gharebagh R, Mostoufi N, Zarghami R, Mahjoob MJ. Nonintrusive characterization of fluidized bed hydrodynamics using vibration signature analysis. *AIChE J*. 2009;56:597–603.
14. Grace JR. Reflections on turbulent fluidization and dense suspension upflow. *Powder Technol*. 2000;113:242–248.
15. van der Stappen MLM, Schouten JC, van den Bleek CM. *Application of deterministic chaos analysis to pressure fluctuation measurements in a 0.96 m^2 CFB riser*. In: Avidan AA, editor. *Circulating Fluidized Bed Technology IV*. New York: AIChE, 1993:54–61.
16. Wu BY, Zhu J, Briens L. A comparison of flow dynamics and flow structure in a riser and a downer. *Chem Eng Technol*. 2007;30:448–459.
17. Taylor EM, Guenther CP, Breault RW. Dynamical tests on fiber optic data taken from the riser section of a circulating fluidized bed. DOE/NETL-IR-2008-045.
18. Song X, Bi HT, Lim CJ, Grace JR, Chan E, Knapper B, McKnight C. Hydrodynamics of the reactor section in fluid cokers. *Powder Technol*. 2004;147:126–136.
19. Briens L, Bojarra M. Monitoring fluidized bed drying of pharmaceutical granules. *AAPS PharmSciTech*. 2010;11:1612–1618.
20. Lee G, Kim S. Pressure fluctuations in turbulent fluidized beds. *J Chem Eng Jpn*. 1988;21:515–521.
21. Manyele SV, Zhu J, Zhang H. Analysis of the microscopic flow structure of a CFB downer reactor using solids concentration signals. *Int J Chem Reactor Eng*. 2003;1:1–17.
22. Breault RW, Casleton EM, Guenther C. Chaotic and statistical tests on fiber optic dynamic data taken from the riser section of a circulating fluidized bed. *Powder Technol*. 2012;220:151–163.
23. Zhang H, Johnston PJ, Zhu J, de Lasa HI, Bergougnou MA. A novel calibration procedure for a fiber optic solids concentration probe. *Powder Technol*. 1998;100:260–272.
24. Zhang H, Zhu J, Bergougnou MA. Hydrodynamics in downflow fluidized beds (1): solids concentration profiles and pressure gradient distributions. *Chem Eng Sci*. 1999;54:5461–5470.
25. Zhang H. Hydrodynamics of a gas–solids downflow fluidized bed reactor, Ph.D. dissertation. London, Ontario: Western University, 1999.
26. Grace JR. *Hydrodynamics of fluidization*. In: Crowe C, editor. *Multiphase Flow Handbook*. New York: CRC Press, 2005:5.55–5.93.
27. Zhu H, Zhu J. New investigation in regime transition from bubbling to turbulent fluidization. *Can J Chem Eng*. 2008;86:553–562.
28. Zhu J, Manyele SV. Radial nonuniformity index (RNI) in fluidized beds and other multiphase flow systems. *Can J Chem Eng*. 2001;79:203–213.
29. Wilhelm RH, Kwauk M. Fluidization of solid particles. *Chem Eng Prog*. 1948;44:201–217.
30. Elnashaie SEH, Grace JR. Complexity, bifurcation and chaos in natural and man-made lumped and distributed systems. *Chem Eng Sci*. 2007;62:3295–3325.
31. Zhu B. Computational modelling and bifurcation analysis of bubbling fluidized processes, Ph.D. dissertation. San Diego: San Diego State University, 2008.
32. Bai D, Zhu J, Jin Y, Yu Z, Internal recirculation flow structure in vertical upward flowing gas–solids suspensions, part I: a core/annular model. *Powder Technol*. 1995;85:171–178.
33. Bi HT, Fan LS. Existence of turbulent regime in gas–solid fluidization. *AIChE J*. 1992;38:297–301.

Manuscript received Apr. 29, 2012, revision received Aug. 5, 2012, and final revision received Oct. 12, 2012.